Effect of flow pulsations on chaos in nanotubes using nonlocal strain gradient theory

Mergen H. Ghayesh [a], Ali Farajpour [a*], Hamed Farokhi [b]

[a] *School of Mechanical Engineering, University of Adelaide, South Australia 5005, Australia*
Email: mergen.ghayesh@adelaide.edu.au (M.H. Ghayesh)
[*] *Corresponding author: ali.farajpourouderji@adelaide.edu.au (A. Farajpour)*
[b] *Department of Mechanical and Construction Engineering, Northumbria University, Newcastle upon Tyne NE1 8ST, UK*
Email: hamed.farokhi@northumbria.ac.uk (H. Farokhi)

Abstract

In this article, a chaos analysis is performed for the viscoelastic nonlinear coupled dynamics of perfectly straight nanotubes conveying pulsatile fluid for the first time. A size-dependent advanced elasticity model is developed with consideration of stress nonlocality as well as the gradient of strain components. After presenting the nonlinear motion equations using Hamilton's approach, they are numerically solved via application of a time-integration technique for a system with a large number of degrees of freedom. Chaos analysis is performed for the nanotube at both subcritical and supercritical flow regimes. Both mean fluid velocity and the amplitude of velocity pulsation are varied as the bifurcation parameter. The proposed size-dependent continuum modelling and numerical results would be useful in order to tailor the system parameters to avoid chaos in nanoelectromechanical devices using fluid-conveying nanotubes.

Keywords: Nanotubes; Flow pulsation; Nonlinear viscoelasticity; Axial inertia; Chaotic response

1. Introduction

Nanoelectromechanical systems (NEMS) have many applications in different fields such as engineering, agriculture and medicine [1, 2]. NEMS-based devices are classified based on various aspects such as geometry, application and manufacturing process. In a class of NEMS-based devices such as nanoresonators and nanogenerators, in which the fundamental part of the system oscillates, understanding the motion of the components of the system becomes important.

Although there are experimental techniques and molecular dynamics (MD) simulations, the size-dependent continuum modelling of nanoscale structural components has attracted increasing attention from researchers [3-7]. The main reasons are that experimental techniques and MD simulations are difficult to perform and computationally costly, respectively. The majority of the size-dependent continuum models have been developed for nano/microbeams [8-10], nano/microshells [11] and nano/microplates [12, 13] as they usually form the structural components of many NEMS-based devices [14-16]. Some important studies in this field are mentioned in the following. The deformation of nanocantilevers was analysed utilising a nonlocal model developed by Peddieson et al. [17]. Tounsi et al. [18] studied thermal and size influences on the wave dispersion characteristics of double-walled nanoscale tubes via the nonlocal theory; they concluded that the results of the local elasticity theory is not reliable for the wave propagation in nanotubes. The vibration of graphene sheets of a sector shape was also investigated using Eringen's theory by Civalek and Akgöz [19]. In another study, Zenkour and Sobhy [20] examined the thermal instability of nanoplates resting on a Winkler-Pasternak substrate; incorporating nonlocal parameter yields a decrease in the critical temperature. Ready [21] also proposed a size-

dependent nonlinear formulation for the static deflection of nonlocal beams and plates. Malekzadeh and Shojaee [22] utilised a nonlocal plate theory with shear, surface and size effects to examine the vibration of plates at nanoscales.

Fluid-conveying tubes at nanoscales have been the focus of recent studies in the field of size-dependent continuum modelling. Soltani et al. [23] developed an Euler-Bernoulli model with size effects for the mechanics of a single nanotube conveying fluid. In an another study, wave dispersion in a double-walled nanotube conveying nanofluid was explored by Wang et al. [24]; they found that size effects should be captured for an accurate estimation of wave propagation characteristics. Liang and Su [25] also developed a continuum model to examine the influence of pulsatile viscous fluid on the instability of nanotubes. Moreover, Filiz and Aydogdu [26] studied the wave dispersion behaviour of fluid-conveying nanotubes with non-homogeneous material properties. In an another investigation by Maraghi et al. [27], the mechanics of fluid-conveying boron nitride nanotubes was analysed. In addition, an elasticity model with size effects was proposed by Amiri et al. [28] for the wave dispersion analysis of nanofluid-conveying nanotubes made of piezoelectric materials. Besides these valuable studies, both linear [29] and nonlinear [30] vibrations of fluid-conveying tubes at nanoscales have been studied employing size-dependent elasticity models. Furthermore, Azrar et al. [31] developed a beam model with nonlocal effects so as to examine the influence of pulsatile flow on the parametric instability of nanotubes. More recently, Atashafrooz et al. [32] has examined nonlocal and strain gradient effects on the linear mechanics of nanofluid-conveying nanotubes; they found that the critical fluid velocity decreases as nonlocal effects become stronger.

In a number of important micro/nanoscale electromechanical systems such as ultrasmall pipettes, biomimetic ultrasmall devices and microfluidic devices, there is an ultrasmall fluid-conveying tube. These systems can be subject to external excitation, and thus chaos may happen. For instance, in microfluidic systems, non-uniform external electromechanical loads are used so as to separate small-scale particles. In these systems, it is very important to adjust the system parameters to avoid chaos. This study paves the way for thoroughly understanding of the chaotic behaviour of fluid-conveying nanotubes subject to flow pulsations.

Table 1 briefly summarises the most relevant studies on the mechanical responses of fluid-conveying nanotubes using size-dependent theories. Scrutinising the available literature on the size-dependent modelling of nanofluid-conveying nanosystems indicates that no nonlinear coupled viscoelastic models have been reported on the chaotic response of nanotubes conveying pulsatile nanofluid (see Table 1). Furthermore, the available nonlinear studies lack two major factors: 1) a through consideration of basis functions, and 2) axial inertia effects. In this paper, this problem is investigated for the first time. Size effects are modelled using a continuum theory incorporating strain gradient and nonlocal influences. The motion equations of the nanotube conveying pulsatile nanofluid are presented via Hamilton's approach incorporating axial inertia. Galerkin's scheme is employed for turning the nonlinear partial differential equations into their ordinary counterparts. Finally, bifurcation results are obtained, and chaotic analysis is performed for the fluid-conveying nanosystem with flow pulsation via help of a time-integration technique. The present continuum modelling would be helpful in designing NEMS-based devices in which nanotubes conveying pulsatile nanofluid are used.

2. A size-dependent nonlinear continuum model for nanotubes conveying pulsatile fluid

In the following, a nonlinear continuum model with both strain gradient and nonlocal effects is proposed for nanotubes conveying pulsatile nanofluid. The influences of viscoelasticity and axial inertia are considered. Figure 1 illustrates the schematic representation of a nanotube conveying pulsatile nanofluid. The geometric properties of the tube are denoted by *L* (length) and *D* (outer diameter).

Euler-Bernoulli assumptions are made in this analysis since the thickness of the nanotube is assumed to be small enough compared to its length. The mathematical formulations are briefly explained in Sections 2 and 3; interested readers are referred to Ref. [33] for more detailed formulations. The strain component (ε_{xx}) incorporating stretching-type nonlinearity is expressed as [34] $\varepsilon_{xx} = 0.5\left(\partial w/\partial x\right)^2 - z\partial^2 w/\partial x^2 + \partial u/\partial x$, in which *w* and *u* represent the transverse deflection and axial displacement of the tube, respectively. The total stress resultants (M_{xx} and N_{xx}) are defined as $M_{xx} = \int_A z t_{xx} dA,\ N_{xx} = \int_A t_{xx} dA,$ where t_{xx} and *A* denote the total stress and tube cross-sectional area, respectively.

Let us assume that l_{sg}, $e_0 a$ and ∇^2 are the strain gradient coefficient, nonlocal coefficient and Laplacian operator, respectively [35-37]. Also, η and *E* are, respectively, the material viscosity and elasticity modulus. The total stress resultants are

$$\begin{aligned}\left[1-\left(e_0 a\right)^2\nabla^2\right]N_{xx} &= \eta A\left(1-l_{sg}^2\nabla^2\right)\left(\frac{\partial w}{\partial x}\frac{\partial^2 w}{\partial t\partial x}+\frac{\partial^2 u}{\partial t\partial x}\right)\\ &+EA\left(1-l_{sg}^2\nabla^2\right)\left[\frac{1}{2}\left(\frac{\partial w}{\partial x}\right)^2+\frac{\partial u}{\partial x}\right],\end{aligned} \tag{1}$$

$$\left[1-\left(e_0 a\right)^2\nabla^2\right]M_{xx}=-\eta I\left(1-l_{sg}^2\nabla^2\right)\frac{\partial^3 w}{\partial t\partial x^2}-EI\left(1-l_{sg}^2\nabla^2\right)\frac{\partial^2 w}{\partial x^2},\tag{2}$$

in which *I* stands for the nanotube second moment of inertia. The elastic energy is given by

$$\begin{aligned}&\delta U_{el}=\int_0^L\int_A\left[\sigma_{xx(el)}^{(1)}\nabla\delta\varepsilon_{xx}+\sigma_{xx(el)}\delta\varepsilon_{xx}\right]dAdx=\\&\left[\int_A\sigma_{xx(el)}^{(1)}\delta\varepsilon_{xx}dA\right]_0^L+\int_0^L\int_A\left[-\nabla\sigma_{xx(el)}^{(1)}\delta\varepsilon_{xx}+\sigma_{xx(el)}\delta\varepsilon_{xx}\right]dAdx\\&=\left[\int_A\sigma_{xx(el)}^{(1)}\delta\varepsilon_{xx}dA\right]_0^L+\int_0^L\int_A\left[t_{xx(el)}\right]\delta\varepsilon_{xx}dAdx,\end{aligned}\tag{3}$$

where $\sigma_{xx(el)}^{(1)}$, ∇ and $\sigma_{xx(el)}$ are the elastic higher-order non-classical stress, gradient operator and elastic zeroth-order non-classical stress, respectively. The nanosystem kinetic energy is expressed as

$$\begin{aligned}&\delta T_k=\int_0^L\left[M\kappa_{nf1}U(t)\frac{\partial u}{\partial t}\frac{\partial\delta u}{\partial x}+M\kappa_{nf1}U(t)\left(1+\frac{\partial u}{\partial x}\right)\frac{\partial\delta u}{\partial t}+m\frac{\partial u}{\partial t}\frac{\partial\delta u}{\partial t}\right]dx\\&+\int_0^L\left[M\left[\kappa_{nf1}U(t)\right]^2\left(1+\frac{\partial u}{\partial x}\right)\frac{\partial\delta u}{\partial x}+M\frac{\partial u}{\partial t}\frac{\partial\delta u}{\partial t}\right]dx\\&+\int_0^L\left[M\kappa_{nf1}U(t)\frac{\partial w}{\partial t}\frac{\partial\delta w}{\partial x}+M\kappa_{nf1}U(t)\frac{\partial w}{\partial x}\frac{\partial\delta w}{\partial t}+m\frac{\partial w}{\partial t}\frac{\partial\delta w}{\partial t}\right]dx\\&+\int_0^L\left[M\left[\kappa_{nf1}U(t)\right]^2\frac{\partial w}{\partial x}\frac{\partial\delta w}{\partial x}+M\frac{\partial w}{\partial t}\frac{\partial\delta w}{\partial t}\right]dx.\end{aligned}\tag{4}$$

In Eq. (4), *m*, κ_{nf1}, *U(t)* and *M* indicate the tube mass per length, velocity correction factor, fluid velocity and fluid mass per length, respectively. The viscous work is expressed as

$$\begin{aligned}&\delta W_{vis}=-\int_0^L\int_A\left[\sigma_{xx(vis)}^{(1)}\nabla\delta\varepsilon_{xx}+\sigma_{xx(vis)}\delta\varepsilon_{xx}\right]dAdx\\&=-\left[\int_A\sigma_{xx(vis)}^{(1)}\delta\varepsilon_{xx}dA\right]_0^L-\int_0^L\int_A\left[t_{xx(vis)}\right]\delta\varepsilon_{xx}dAdx,\end{aligned}\tag{5}$$

where $\sigma_{xx(vis)}^{(1)}$ and $\sigma_{xx(vis)}$ are the viscoelastic higher-order non-classical stress and viscoelastic zeroth-order non-classical stress, respectively.

Hamilton's approach for deriving the equations of motion is expressed as

$$\int_{t_1}^{t_2}\left[\delta W_{vis}-\delta U_{el}+\delta T_k\right]\mathrm{d}t=0. \tag{6}$$

It is assumed that the fluid velocity varies versus time according to the following relation

$$U=U_0+U_1\cos\left(\omega_f t\right), \tag{7}$$

where U_0, U_1 and ω_f indicate the mean velocity, the amplitude of the fluid velocity and pulsation frequency, respectively. The fluid velocity profile is assumed to follow Eq. (7) due to the fact that this equation represents a typical pulsatile flow. Other profiles can be also considered in a similar way; however, this velocity profile is the most popular one. The first term of the profile (i.e. U_0) represents the mean fluid speed while the second term denotes the velocity pulsation.

In the present formulation, the following non-dimensional parameters are used

$$\begin{aligned}
&w^*=\frac{w}{D},\ s=\frac{L}{D},\ x^*=\frac{x}{L},\ u^*=\frac{u}{D},\ \bar{\nabla}^2=\frac{\partial^2}{\partial x^{*2}},\ \chi_{sg}=\frac{l_{sg}}{L},\\
&\chi_{nl}=\frac{e_0 a}{L},\ \bar{M}=\frac{M}{M+m},\ \Xi=\frac{AL^2}{I},\ t^*=\frac{t}{L^2}\left(\frac{EI}{m+M}\right)^{\frac{1}{2}},\\
&U^*=LU\left(\frac{M}{EI}\right)^{\frac{1}{2}},\ U_0^*=LU_0\left(\frac{M}{EI}\right)^{\frac{1}{2}},\ U_1^*=LU_1\left(\frac{M}{EI}\right)^{\frac{1}{2}},\\
&\eta^*=\frac{\eta}{EL^2}\left(\frac{EI}{m+M}\right)^{\frac{1}{2}},\ \omega_f^*=L^2\omega_f\left(\frac{m+M}{EI}\right)^{\frac{1}{2}}.
\end{aligned} \tag{8}$$

Using Eq. (7) together with the non-dimensional parameters defined in the above equation (i.e. Eq. (8)), the governing equations can be written as

$$
\begin{aligned}
&\frac{s}{\Xi}\left(\frac{\partial^2 u}{\partial t^2}+2\kappa_{nf1}\sqrt{\bar{M}}\left[U_0+U_1\cos\left(\omega_f t\right)\right]\frac{\partial^2 u}{\partial t\partial x}\right.\\
&+\left(\kappa_{nf1}\right)^2\left[U_0+U_1\cos\left(\omega_f t\right)\right]^2\frac{\partial^2 u}{\partial x^2}\\
&\left.-\kappa_{nf1}\sqrt{\bar{M}}\omega_f U_1\sin\left(\omega_f t\right)\left(s+\frac{\partial u}{\partial x}\right)\right)\\
&-\frac{s}{\Xi}\chi_{nl}^2\frac{\partial^2}{\partial x^2}\left(\frac{\partial^2 u}{\partial t^2}+2\kappa_{nf1}\sqrt{\bar{M}}\left[U_0+U_1\cos\left(\omega_f t\right)\right]\frac{\partial^2 u}{\partial t\partial x}\right.\\
&+\left(\kappa_{nf1}\right)^2\left[U_0+U_1\cos\left(\omega_f t\right)\right]^2\frac{\partial^2 u}{\partial x^2}\\
&\left.-\kappa_{nf1}\sqrt{\bar{M}}\omega_f U_1\sin\left(\omega_f t\right)\left(s+\frac{\partial u}{\partial x}\right)\right)\\
&-\frac{\partial}{\partial x}\left(\frac{1}{2}\left(\frac{\partial w}{\partial x}\right)^2+s\frac{\partial u}{\partial x}\right)+\chi_{sg}^2\frac{\partial^3}{\partial x^3}\left(\frac{1}{2}\left(\frac{\partial w}{\partial x}\right)^2+s\frac{\partial u}{\partial x}\right)\\
&-\eta\frac{\partial}{\partial x}\left(\frac{\partial w}{\partial x}\frac{\partial^2 w}{\partial t\partial x}+s\frac{\partial^2 u}{\partial t\partial x}\right)+\eta\chi_{sg}^2\frac{\partial^3}{\partial x^3}\left(\frac{\partial w}{\partial x}\frac{\partial^2 w}{\partial t\partial x}+s\frac{\partial^2 u}{\partial t\partial x}\right)=0,
\end{aligned}
\tag{9}
$$

$$
\begin{aligned}
&\frac{\partial^2 w}{\partial t^2}+2\kappa_{nf1}\sqrt{\bar{M}}\left[U_0+U_1\cos\left(\omega_f t\right)\right]\frac{\partial^2 w}{\partial t\partial x}\\
&+\left(\kappa_{nf1}\right)^2\left[U_0+U_1\cos\left(\omega_f t\right)\right]^2\frac{\partial^2 w}{\partial x^2}-\kappa_{nf1}\sqrt{\bar{M}}\omega_f U_1\sin\left(\omega_f t\right)\frac{\partial w}{\partial x}\\
&-\chi_{nl}^2\frac{\partial^2}{\partial x^2}\left(\frac{\partial^2 w}{\partial t^2}+2\kappa_{nf1}\sqrt{\bar{M}}\left[U_0+U_1\cos\left(\omega_f t\right)\right]\frac{\partial^2 w}{\partial t\partial x}\right.\\
&\left.+\left(\kappa_{nf1}\right)^2\left[U_0+U_1\cos\left(\omega_f t\right)\right]^2\frac{\partial^2 w}{\partial x^2}-\kappa_{nf1}\sqrt{\bar{M}}\omega_f U_1\sin\left(\omega_f t\right)\frac{\partial w}{\partial x}\right)\\
&+\eta\frac{\partial^5 w}{\partial t\partial x^4}-\eta\chi_{sg}^2\frac{\partial^7 w}{\partial t\partial x^6}+\frac{\partial^4 w}{\partial x^4}-\chi_{sg}^2\frac{\partial^6 w}{\partial x^6}\\
&-\frac{\Xi}{s^2}\frac{\partial}{\partial x}\left[\left(s\frac{\partial u}{\partial x}+\frac{1}{2}\left(\frac{\partial w}{\partial x}\right)^2\right)\frac{\partial w}{\partial x}-\chi_{sg}^2\left\{\frac{\partial^2}{\partial x^2}\left(s\frac{\partial u}{\partial x}+\frac{1}{2}\left(\frac{\partial w}{\partial x}\right)^2\right)\right\}\frac{\partial w}{\partial x}\right.\\
&+\eta\frac{\partial w}{\partial x}\left(\frac{\partial w}{\partial x}\frac{\partial^2 w}{\partial t\partial x}+s\frac{\partial^2 u}{\partial t\partial x}\right)-\chi_{sg}^2\eta\frac{\partial w}{\partial x}\frac{\partial^2}{\partial x^2}\left(\frac{\partial w}{\partial x}\frac{\partial^2 w}{\partial t\partial x}+s\frac{\partial^2 u}{\partial t\partial x}\right)\\
&+\frac{s}{\Xi}\chi_{nl}^2\frac{\partial w}{\partial x}\left(\frac{\partial^3 u}{\partial x\partial t^2}+2\kappa_{nf1}\sqrt{\bar{M}}\left[U_0+U_1\cos\left(\omega_f t\right)\right]\frac{\partial^3 u}{\partial t\partial x^2}\right.\\
&\left.\left.+\left(\kappa_{nf1}\right)^2\left[U_0+U_1\cos\left(\omega_f t\right)\right]^2\frac{\partial^3 u}{\partial x^3}-\kappa_{nf1}\sqrt{\bar{M}}\omega_f U_1\sin\left(\omega_f t\right)\frac{\partial^2 u}{\partial x^2}\right)\right]
\end{aligned}
$$

$$
\begin{aligned}
&+\frac{\Xi}{s^2}\chi_{nl}^2\frac{\partial^3}{\partial x^3}\left[\frac{\partial w}{\partial x}\left(\frac{1}{2}\left(\frac{\partial w}{\partial x}\right)^2+s\frac{\partial u}{\partial x}\right)-\chi_{sg}^2\frac{\partial w}{\partial x}\frac{\partial^2}{\partial x^2}\left(\frac{1}{2}\left(\frac{\partial w}{\partial x}\right)^2+s\frac{\partial u}{\partial x}\right)\right.\\
&+\eta\frac{\partial w}{\partial x}\left(s\frac{\partial^2 u}{\partial t\partial x}+\frac{\partial w}{\partial x}\frac{\partial^2 w}{\partial t\partial x}\right)-\eta\chi_{sg}^2\frac{\partial w}{\partial x}\frac{\partial^2}{\partial x^2}\left(s\frac{\partial^2 u}{\partial t\partial x}+\frac{\partial w}{\partial x}\frac{\partial^2 w}{\partial t\partial x}\right)\\
&+\frac{s}{\Xi}\chi_{nl}^2\frac{\partial w}{\partial x}\left(\frac{\partial^3 u}{\partial x\partial t^2}+2\kappa_{nf1}\sqrt{\bar{M}}\left[U_0+U_1\cos\left(\omega_f t\right)\right]\frac{\partial^3 u}{\partial t\partial x^2}\right.\\
&\left.\left.+\left(\kappa_{nf1}\right)^2\left[U_0+U_1\cos\left(\omega_f t\right)\right]^2\frac{\partial^3 u}{\partial x^3}-\kappa_{nf1}\sqrt{\bar{M}}\omega_f U_1\sin\left(\omega_f t\right)\frac{\partial^2 u}{\partial x^2}\right)\right]=0.
\end{aligned}
\tag{10}
$$

Equations (9) and (10) describe the nonlinear bifurcation behaviour of nanotubes conveying pulsatile nanofluid; the influences of stress nonlocality, strain gradients and slip conditions are incorporated. It should be noticed that slip conditions are incorporated via the following velocity correction factor [32]

$$
\kappa_{nf1}=\left(1+\frac{4\left(2-\sigma_v\right)Kn}{\sigma_v\left(1-\beta Kn\right)}\right)\left(1+\lambda Kn\right),
\tag{11}
$$

where

$$
\lambda=\frac{2\lambda_0}{\pi}\tan^{-1}\left(\alpha_0\left(Kn\right)^{\alpha_1}\right).
\tag{12}
$$

in which $\lambda_0=64\beta/\left[3\pi\left(\beta-4\right)\right]$. Also, β and σ_v are constant coefficients, which are obtained as $\beta=-1$ and $\sigma_v=0.7$ for fluid-conveying nanotubes. In Eq. (12), the constant coefficients are given by $\alpha_0=4$ and $\alpha_1=0.4$.

3. Numerical solution method

To make the solution procedure easier, the coupled differential equations of the nanosystem (i.e. Eqs. (9) and (10)) are discretised using the following relations [38]

$$u=\sum_{j=1}^{N_1}\Psi_j(x)r_j(t),$$
$$w=\sum_{j=1}^{N_2}\Phi_j(x)q_j(t), \tag{13}$$

Here (N_1,N_2)=the number of basis functions along (x,z); (Ψ_j,Φ_j)=the basis functions for (u,w); (r_j,q_j)=the generalised coordinates for (u,w) [39, 40]. Substituting Eq. (13) into Eqs. (9) and (10) gives the following discretised equations for the nonlinear coupled bifurcation behaviour of nanotubes conveying pulsatile nanofluid

$$\begin{aligned}
&\int_0^1\left\{\frac{s}{\Xi}\Psi_k\left(\sum_{j=1}^{N_1}\Psi_j\frac{d^2r_j}{dt^2}+2\kappa_{nf1}\sqrt{\bar{M}}\left[U_0+U_1\cos\left(\omega_f t\right)\right]\sum_{j=1}^{N_1}\frac{d\Psi_j}{\partial x}\frac{dr_j}{dt}\right.\right.\\
&+\left(\kappa_{nf1}\right)^2\left[U_0+U_1\cos\left(\omega_f t\right)\right]^2\sum_{j=1}^{N_1}\frac{d^2\Psi_j}{dx^2}r_j\\
&\left.\left.-\kappa_{nf1}\sqrt{\bar{M}}\omega_f U_1\sin\left(\omega_f t\right)\left(s+\sum_{j=1}^{N_1}\frac{d\Psi_j}{dx}r_j\right)\right)\right\}dx\\
&-\int_0^1\left\{\frac{s}{\Xi}\chi_{nl}^2\Psi_k\frac{d^2}{dx^2}\left(+2\kappa_{nf1}\sqrt{\bar{M}}\left[U_0+U_1\cos\left(\omega_f t\right)\right]\sum_{j=1}^{N_1}\frac{d\Psi_j}{\partial x}\frac{dr_j}{dt}\right.\right.\\
&+\sum_{j=1}^{N_1}\Psi_j\frac{d^2r_j}{dt^2}+\left(\kappa_{nf1}\right)^2\left[U_0+U_1\cos\left(\omega_f t\right)\right]^2\sum_{j=1}^{N_1}\frac{d^2\Psi_j}{dx^2}r_j\\
&\left.\left.-\kappa_{nf1}\sqrt{\bar{M}}\omega_f U_1\sin\left(\omega_f t\right)\left(s+\sum_{j=1}^{N_1}\frac{d\Psi_j}{dx}r_j\right)\right)\right\}dx\\
&-\int_0^1\left\{\Psi_k\frac{d}{dx}\left(\frac{1}{2}\sum_{i=1}^{N_2}\sum_{j=1}^{N_2}\frac{d\Phi_i}{dx}\frac{d\Phi_j}{dx}q_iq_j+s\sum_{j=1}^{N_1}\frac{d\Psi_j}{dx}r_j\right)\right\}dx\\
&+\int_0^1\left\{\chi_{sg}^2\Psi_k\frac{d^3}{dx^3}\left(\frac{1}{2}\sum_{i=1}^{N_2}\sum_{j=1}^{N_2}\frac{d\Phi_i}{dx}\frac{d\Phi_j}{dx}q_iq_j+s\sum_{j=1}^{N_1}\frac{d\Psi_j}{dx}r_j\right)\right\}dx\\
&-\int_0^1\left\{\eta\Psi_k\frac{d}{dx}\left(\sum_{i=1}^{N_2}\sum_{j=1}^{N_2}\frac{d\Phi_i}{dx}\frac{d\Phi_j}{dx}\frac{dq_j}{dt}q_i+s\sum_{j=1}^{N_1}\frac{d\Psi_j}{\partial x}\frac{dr_j}{dt}\right)\right\}dx\\
&+\int_0^1\left\{\eta\chi_{sg}^2\Psi_k\frac{d^3}{dx^3}\left(\sum_{i=1}^{N_2}\sum_{j=1}^{N_2}\frac{d\Phi_i}{dx}\frac{d\Phi_j}{dx}\frac{dq_j}{dt}q_i+s\sum_{j=1}^{N_1}\frac{d\Psi_j}{\partial x}\frac{dr_j}{dt}\right)\right\}dx=0,
\end{aligned} \tag{14}$$

$$\int_0^1 \left\{ \Phi_l \left(\sum_{j=1}^{N_2} \Phi_j \frac{d^2 q_j}{dt^2} + 2\kappa_{nf1} \sqrt{\bar{M}} \left[U_0 + U_1 \cos\left(\omega_f t\right) \right] \sum_{j=1}^{N_2} \frac{d\Phi_j}{dx} \frac{dq_j}{dt} \right.\right.$$

$$\left.\left. + \left(\kappa_{nf1}\right)^2 \left[U_0 + U_1 \cos\left(\omega_f t\right) \right]^2 \sum_{j=1}^{N_2} \frac{d^2 \Phi_j}{dx^2} q_j - \kappa_{nf1} \sqrt{\bar{M}} \omega_f U_1 \sin\left(\omega_f t\right) \sum_{j=1}^{N_2} \frac{d\Phi_j}{dx} q_j \right) \right\} dx$$

$$- \int_0^1 \left\{ \Phi_l \chi_{nl}^2 \frac{d^2}{dx^2} \left(\sum_{j=1}^{N_2} \Phi_j \frac{d^2 q_j}{dt^2} + 2\kappa_{nf1} \sqrt{\bar{M}} \left[U_0 + U_1 \cos\left(\omega_f t\right) \right] \sum_{j=1}^{N_2} \frac{d\Phi_j}{dx} \frac{dq_j}{dt} \right.\right.$$

$$\left.\left. + \left(\kappa_{nf1}\right)^2 \left[U_0 + U_1 \cos\left(\omega_f t\right) \right]^2 \sum_{j=1}^{N_2} \frac{d^2 \Phi_j}{dx^2} q_j - \kappa_{nf1} \sqrt{\bar{M}} \omega_f U_1 \sin\left(\omega_f t\right) \sum_{j=1}^{N_2} \frac{d\Phi_j}{dx} q_j \right) \right\} dx$$

$$+ \int_0^1 \left\{ \Phi_l \left(\eta \sum_{j=1}^{N_2} \frac{d^4 \Phi_j}{dx^4} \frac{dq_j}{dt} - \eta \chi_{sg}^2 \sum_{j=1}^{N_2} \frac{d^6 \Phi_j}{dx^6} \frac{dq_j}{dt} + \sum_{j=1}^{N_2} \frac{d^4 \Phi_j}{dx^4} q_j - \chi_{sg}^2 \sum_{j=1}^{N_2} \frac{d^6 \Phi_j}{dx^6} q_j \right) \right\} dx$$

$$- \int_0^1 \left\{ \frac{\Xi}{s^2} \Phi_l \frac{d}{dx} \left[\left(\sum_{k=1}^{N_2} \frac{d\Phi_k}{dx} q_k \right) \left(\frac{1}{2} \sum_{i=1}^{N_2} \sum_{j=1}^{N_2} \frac{d\Phi_i}{dx} \frac{d\Phi_j}{dx} q_i q_j + s \sum_{j=1}^{N_1} \frac{d\Psi_j}{dx} r_j \right) \right.\right.$$

$$- \chi_{sg}^2 \left(\sum_{k=1}^{N_2} \frac{d\Phi_k}{dx} q_k \right) \frac{d^2}{dx^2} \left(\frac{1}{2} \sum_{i=1}^{N_2} \sum_{j=1}^{N_2} \frac{d\Phi_i}{dx} \frac{d\Phi_j}{dx} q_i q_j + s \sum_{j=1}^{N_1} \frac{d\Psi_j}{dx} r_j \right)$$

$$+ \eta \left(\sum_{k=1}^{N_2} \frac{d\Phi_k}{dx} q_k \right) \left(\sum_{i=1}^{N_2} \sum_{j=1}^{N_2} \frac{d\Phi_i}{dx} \frac{d\Phi_j}{dx} \frac{dq_j}{dt} q_i + s \sum_{j=1}^{N_1} \frac{d\Psi_j}{\partial x} \frac{dr_j}{dt} \right)$$

$$- \chi_{sg}^2 \eta \left(\sum_{k=1}^{N_2} \frac{d\Phi_k}{dx} q_k \right) \frac{d^2}{dx^2} \left(\sum_{i=1}^{N_2} \sum_{j=1}^{N_2} \frac{d\Phi_i}{dx} \frac{d\Phi_j}{dx} \frac{dq_j}{dt} q_i + s \sum_{j=1}^{N_1} \frac{d\Psi_j}{\partial x} \frac{dr_j}{dt} \right)$$

$$+ \frac{s}{\Xi} \chi_{nl}^2 \left(\sum_{k=1}^{N_2} \frac{d\Phi_k}{dx} q_k \right) \left(\sum_{j=1}^{N_1} \frac{d\Psi_j}{\partial x} \frac{d^2 r_j}{dt^2} + 2\kappa_{nf1} \sqrt{\bar{M}} \left[U_0 + U_1 \cos\left(\omega_f t\right) \right] \sum_{j=1}^{N_1} \frac{d^2 \Psi_j}{\partial x^2} \frac{dr_j}{dt} \right.$$

$$\left.\left.\left. + \left(\kappa_{nf1}\right)^2 \left[U_0 + U_1 \cos\left(\omega_f t\right) \right]^2 \sum_{j=1}^{N_1} \frac{d^3 \Psi_j}{\partial x^3} r_j - \kappa_{nf1} \sqrt{\bar{M}} \omega_f U_1 \sin\left(\omega_f t\right) \sum_{j=1}^{N_1} \frac{d^2 \Psi_j}{\partial x^2} r_j \right) \right] \right\} dx$$

$$+ \int_0^1 \left\{ \frac{\Xi}{s^2} \chi_{nl}^2 \Phi_l \frac{d^3}{dx^3} \left[\left(\sum_{k=1}^{N_2} \frac{d\Phi_k}{dx} q_k \right) \left(\frac{1}{2} \sum_{i=1}^{N_2} \sum_{j=1}^{N_2} \frac{d\Phi_i}{dx} \frac{d\Phi_j}{dx} q_i q_j + s \sum_{j=1}^{N_1} \frac{d\Psi_j}{dx} r_j \right) \right.\right.$$

$$- \chi_{sg}^2 \left(\sum_{k=1}^{N_2} \frac{d\Phi_k}{dx} q_k \right) \frac{d^2}{dx^2} \left(\frac{1}{2} \sum_{i=1}^{N_2} \sum_{j=1}^{N_2} \frac{d\Phi_i}{dx} \frac{d\Phi_j}{dx} q_i q_j + s \sum_{j=1}^{N_1} \frac{d\Psi_j}{dx} r_j \right)$$

$$+ \eta \left(\sum_{k=1}^{N_2} \frac{d\Phi_k}{dx} q_k \right) \left(\sum_{i=1}^{N_2} \sum_{j=1}^{N_2} \frac{d\Phi_i}{dx} \frac{d\Phi_j}{dx} \frac{dq_j}{dt} q_i + s \sum_{j=1}^{N_1} \frac{d\Psi_j}{\partial x} \frac{dr_j}{dt} \right)$$

$$- \eta \chi_{sg}^2 \left(\sum_{k=1}^{N_2} \frac{d\Phi_k}{dx} q_k \right) \frac{d^2}{dx^2} \left(\sum_{i=1}^{N_2} \sum_{j=1}^{N_2} \frac{d\Phi_i}{dx} \frac{d\Phi_j}{dx} \frac{dq_j}{dt} q_i + s \sum_{j=1}^{N_1} \frac{d\Psi_j}{\partial x} \frac{dr_j}{dt} \right)$$

$$+\frac{s}{\Xi}\chi_{nl}^2\left(\sum_{k=1}^{N_2}\frac{d\Phi_k}{dx}q_k\right)\left(\sum_{j=1}^{N_1}\frac{d\Psi_j}{\partial x}\frac{d^2r_j}{dt^2}+2\kappa_{nf1}\sqrt{\bar{M}}\left[U_0+U_1\cos\left(\omega_f t\right)\right]\sum_{j=1}^{N_1}\frac{d^2\Psi_j}{\partial x^2}\frac{dr_j}{dt}\right.$$
$$\left.+\left(\kappa_{nf1}\right)^2\left[U_0+U_1\cos\left(\omega_f t\right)\right]^2\sum_{j=1}^{N_1}\frac{d^3\Psi_j}{\partial x^3}r_j-\kappa_{nf1}\sqrt{\bar{M}}\omega_f U_1\sin\left(\omega_f t\right)\sum_{j=1}^{N_1}\frac{d^2\Psi_j}{\partial x^2}r_j\right)\Bigg]\Bigg\}dx=0. \quad (15)$$

It is assumed that the nanoscale tube is clamped at both ends. To determine the bifurcation behaviour of the nanosystem, a direct time-integration technique is applied to the above coupled ordinary differential equations.

4. Results and discussion

In this section, the effects of flow pulsation on the bifurcation behaviour of nanotubes are analysed through different examples. The mechanical properties of the nanotube are taken as v=0.3, E=610 MPa and ρ_t=1024 kg/m^3 in which v, E and ρ_t are, respectively, Poisson's ratio, elasticity constant and density of the tube [41, 42]. The outer radius, thickness and length-to-diameter ratio are as R_{out} =290.5 nm, h=66.0 nm and L/d_{out} =20, respectively. Furthermore, the Knudsen number, velocity correction factor and dimensionless mass ratio are as Kn=0.015, κ_{nf1}=1.119 and $\bar{M}$=0.5915, respectively [29]. The dimensionless geometrical properties and scale coefficients are given by (s=20.0, Ξ =4006.94) and ($\chi_{sg}=0.04$, $\chi_{nl}=0.09$), respectively. In the numerical solution, 20 degrees of freedom are assumed (10 for u and 10 for w), leading to a converged solution.

4.1. U_0 *as the bifurcation parameter*

The pulsatile fluid depends on two different velocity factors: 1) the mean velocity, and 2) the amplitude of fluid velocity. In this subsection, the mean fluid velocity is varied as the bifurcation parameter. Figure 2 indicates the bifurcations for a nanotube conveying fluid

without pulsation (U_1=0). The nanotube itself is assumed to be viscoelastic so as to take into account the effects of internal energy loss. The vertical axis of the diagram shows the transverse deflection at x=0.5. The unstable configuration is also plotted in Fig. 2 (dashed line). The dimensionless critical velocity related to static instability, in which the transverse deflection starts growing, is 4.99989.

The bifurcation diagram of nanotubes conveying pulsatile fluid for motions in z direction is indicated in Fig. 3 for ω_f = 5.00 and U_1= 0.05U_0. The only difference between Figs. 2 and 3 is in the value of U_1. Comparing Fig. 2 to Fig. 3 indicates that the bifurcation behaviour of the nanotube conveying nanofluid with constant velocity is completely different from the case with flow pulsation. Only 5% flow velocity variation changes the nanosystem behaviour significantly and even causes chaotic motion. In addition, the critical fluid velocity of the system related to instability is lower than the case without pulsation.

In Fig. 4, the bifurcation behaviour of nanotubes conveying pulsatile fluid is indicated; this time, the pulsation frequency and the amplitude of the fluid velocity are taken as ω_f = 5.00 and U_1=0.10U_0, respectively. It is observed that the bifurcation behaviour of the fluid-conveying nanotube is very sensitive to the nanofluid velocity variation. Only 5% increase in the amplitude of the fluid velocity with respect to the previous case illustrated in Fig. 3, yields a significant change in the bifurcation response. The chaotic regions are noticeably increased when U_1 increases. In addition, increasing the amplitude of the nanofluid velocity decreases the critical velocity related to instability. For clarification, the detail of the system chaotic behaviour of Fig. 4 at U_0=5.94 is given in Fig. 5 for both motions in x and z directions.

4.2. U_1 *as the bifurcation parameter*

In the following subsection, the fluid velocity amplitude plays the role of the bifurcation parameter. Figures 6(a) and 6(b) depict the bifurcation behaviour of nanotubes conveying fluid with pulsation for the motions in *z* and *x* directions, respectively. The mean fluid velocity is set to U_0 = 4.92. Since the mean velocity is lower than the critical velocity, the nanosystem operates at the subcritical regime. For sufficiently small values of U_1 (i.e. less than 0.01), a periodic motion is found for the system. Nonetheless, the viscoelastic nanotube displays a period-2 motion as a small increase in U_1 is imposed on the nanosystem. The period-2 motion is valid until U_1 =0.1435 in which the motion type turns into a period-4 type. Different motion types are also seen from Fig. 6 as U_1 is further increased. For clarification, the details of the period-2 and period-4 motions of Fig. 6 at U_1 =0.1 and U_1 =0.15 are, respectively, plotted in Figs. 7 and 8, respectively.

Subcritical bifurcation responses for the nanotube conveying pulsatile nanofluid for motions in *z* and *x* directions are, respectively, shown in Figs. 9(a) and 9(b); these diagrams are plotted for U_0 = 4.96. Comparing Fig. 9 to Fig. 6 reveals that a bit increase in the mean velocity in the subcritical regime results in a considerable change in the bifurcation behaviour. Near the critical point related to instability, the bifurcation behaviour turns into chaos with increasing the fluid mean velocity. The chaotic response occurs when the non-dimensional amplitude of the nanofluid velocity is in the range of 0.2-0.3. The detail of the chaotic response of the system at U_1 = 0.25 is shown in Fig. 10.

Figures 11 and 12 depict the supercritical bifurcation of nanotubes conveying pulsatile fluid for U_0=5.02 and U_0=5.06, respectively. It can be concluded that the supercritical response of the nanotube with viscoelastic properties subject to fluid pulsation is

dominated by chaos close to the critical point. However, a slight increase in the value of the mean velocity noticeably reduces chaotic response in the viscoelastic nanotube for motions in both directions.

5. Conclusions

A nonlinear coupled continuum model has been developed to analyse chaos in fluid-conveying nanotubes with flow pulsation. The influences of viscoelasticity as well as axial inertia effects were taken into consideration. A combination of nonlocal theory and the theory of strain gradient was utilised to model size effects. The size-dependent nonlinear partial differential equations were obtained via help of Hamilton's approach. After discretising the nonlinear equations using Galerkin's technique, they were numerically solved via a time-integration method.

From numerical results, it was observed that the chaotic response of the nanotube conveying nanofluid with constant velocity is substantially different from that of flow pulsation. The critical fluid velocity in the case with flow pulsation is lower than the case without pulsation. Both mean fluid velocity and the amplitude of velocity variation have a significant role to play in the chaotic behaviour of the fluid-conveying nanotube. Furthermore, it was found that near the critical point, the subcritical response of the nanosystem turns into chaos with a slight increase in the fluid mean velocity. Nonetheless, a small increase in the value of the mean velocity substantially decreases chaos in the supercritical nonlinear dynamic response of the viscoelastic nanotube conveying pulsatile nanofluid.

Declarations of interest: none.

Appendix A

To show the validity of the present model, the calculated results are compared to those determined via experimental measurement in Table 2. The experimental results were extracted by Garcia-Sanchez et al. [43] using a scanning force microscopy method. Young's modulus, density and boundary conditions of the elastic nanotube without fluid flow are taken as 1 TPa, 2200 kg/m^3 and clamped-clamped, respectively. The results calculated using both classical and size-dependent theories are provided in the table. It is observed that compared to the classical theory, the results of the size-dependent theory are in a reasonable agreement with those of experimental measurement. The appropriate scale parameters for each length and radius are also listed in the table.

References

[1] J. Cha, K.W. Kim, C. Daraio, Experimental realization of on-chip topological nanoelectromechanical metamaterials, Nature, 564 (2018) 229.
[2] X. Feng, C. White, A. Hajimiri, M.L. Roukes, A self-sustaining ultrahigh-frequency nanoelectromechanical oscillator, Nature nanotechnology, 3 (2008) 342.
[3] F. Tajaddodianfar, H.N. Pishkenari, M.R.H. Yazdi, Prediction of chaos in electrostatically actuated arch micro-nano resonators: Analytical approach, Communications in Nonlinear Science and Numerical Simulation, 30 (2016) 182-195.
[4] H. Dai, L. Wang, Size-dependent pull-in voltage and nonlinear dynamics of electrically actuated microcantilever-based MEMS: A full nonlinear analysis, Communications in Nonlinear Science and Numerical Simulation, 46 (2017) 116-125.
[5] M.H. Ghayesh, H. Farokhi, A. Farajpour, Chaotic oscillations of viscoelastic microtubes conveying pulsatile fluid, Microfluidics and Nanofluidics, 22 (2018) 72.
[6] R. Ansari, S. Sahmani, Small scale effect on vibrational response of single-walled carbon nanotubes with different boundary conditions based on nonlocal beam models, Communications in Nonlinear Science and Numerical Simulation, 17 (2012) 1965-1979.
[7] H. Farokhi, M.P. Païdoussis, A.K. Misra, Nonlinear behaviour and mass detection sensitivity of geometrically imperfect cantilevered carbon nanotube resonators, Communications in Nonlinear Science and Numerical Simulation, 65 (2018) 272-298.
[8] A.E. Abouelregal, A.M. Zenkour, Nonlocal thermoelastic model for temperature-dependent thermal conductivity nanobeams due to dynamic varying loads, Microsystem Technologies, 24 (2018) 1189-1199.
[9] M.H. Ghayesh, H. Farokhi, S. Hussain, Viscoelastically coupled size-dependent dynamics of microbeams, International Journal of Engineering Science, 109 (2016) 243-255.
[10] H. Farokhi, M.H. Ghayesh, A. Gholipour, S. Hussain, Motion characteristics of bilayered extensible Timoshenko microbeams, International Journal of Engineering Science, 112 (2017) 1-17.
[11] M.H. Ghayesh, H. Farokhi, Nonlinear mechanics of doubly curved shallow microshells, International Journal of Engineering Science, 119 (2017) 288-304.
[12] M. Farajpour, A. Shahidi, A. Farajpour, A nonlocal continuum model for the biaxial buckling analysis of composite nanoplates with shape memory alloy nanowires, Materials Research Express, 5 (2018) 035026.
[13] H. Farokhi, M.H. Ghayesh, Nonlinear mechanics of electrically actuated microplates, International Journal of Engineering Science, 123 (2018) 197-213.
[14] S.B. Sassi, F. Najar, Strong nonlinear dynamics of MEMS and NEMS structures based on semi-analytical approaches, Communications in Nonlinear Science and Numerical Simulation, 61 (2018) 1-21.
[15] D.I. Caruntu, R. Oyervides, Frequency response reduced order model of primary resonance of electrostatically actuated MEMS circular plate resonators, Communications in Nonlinear Science and Numerical Simulation, 43 (2017) 261-270.
[16] F. Lakrad, M. Belhaq, Suppression of pull-in instability in MEMS using a high-frequency actuation, Communications in Nonlinear Science and Numerical Simulation, 15 (2010) 3640-3646.
[17] J. Peddieson, G.R. Buchanan, R.P. McNitt, Application of nonlocal continuum models to nanotechnology, International Journal of Engineering Science, 41 (2003) 305-312.
[18] A. Tounsi, H. Heireche, H. Berrabah, A. Benzair, L. Boumia, Effect of small size on wave propagation in double-walled carbon nanotubes under temperature field, Journal of Applied Physics, 104 (2008) 104301.
[19] Ö. Civalek, B. Akgöz, Vibration analysis of micro-scaled sector shaped graphene surrounded by an elastic matrix, Computational Materials Science, 77 (2013) 295-303.

[20] A. Zenkour, M. Sobhy, Nonlocal elasticity theory for thermal buckling of nanoplates lying on Winkler–Pasternak elastic substrate medium, Physica E: Low-dimensional Systems and Nanostructures, 53 (2013) 251-259.
[21] J. Reddy, Nonlocal nonlinear formulations for bending of classical and shear deformation theories of beams and plates, International Journal of Engineering Science, 48 (2010) 1507-1518.
[22] P. Malekzadeh, M. Shojaee, A two-variable first-order shear deformation theory coupled with surface and nonlocal effects for free vibration of nanoplates, Journal of Vibration and Control, 21 (2015) 2755-2772.
[23] P. Soltani, M. Taherian, A. Farshidianfar, Vibration and instability of a viscous-fluid-conveying single-walled carbon nanotube embedded in a visco-elastic medium, Journal of Physics D: Applied Physics, 43 (2010) 425401.
[24] Y.-Z. Wang, F.-M. Li, K. Kishimoto, Wave propagation characteristics in fluid-conveying double-walled nanotubes with scale effects, Computational Materials Science, 48 (2010) 413-418.
[25] F. Liang, Y. Su, Stability analysis of a single-walled carbon nanotube conveying pulsating and viscous fluid with nonlocal effect, Applied Mathematical Modelling, 37 (2013) 6821-6828.
[26] S. Filiz, M. Aydogdu, Wave propagation analysis of embedded (coupled) functionally graded nanotubes conveying fluid, Composite Structures, 132 (2015) 1260-1273.
[27] Z.K. Maraghi, A.G. Arani, R. Kolahchi, S. Amir, M. Bagheri, Nonlocal vibration and instability of embedded DWBNNT conveying viscose fluid, Composites Part B: Engineering, 45 (2013) 423-432.
[28] A. Amiri, R. Talebitooti, L. Li, Wave propagation in viscous-fluid-conveying piezoelectric nanotubes considering surface stress effects and Knudsen number based on nonlocal strain gradient theory, The European Physical Journal Plus, 133 (2018) 252.
[29] R. Bahaadini, A.R. Saidi, M. Hosseini, On dynamics of nanotubes conveying nanoflow, International Journal of Engineering Science, 123 (2018) 181-196.
[30] H. Askari, E. Esmailzadeh, Forced vibration of fluid conveying carbon nanotubes considering thermal effect and nonlinear foundations, Composites Part B: Engineering, 113 (2017) 31-43.
[31] A. Azrar, L. Azrar, A. Aljinaidi, Numerical modeling of dynamic and parametric instabilities of single-walled carbon nanotubes conveying pulsating and viscous fluid, Composite Structures, 125 (2015) 127-143.
[32] M. Atashafrooz, R. Bahaadini, H.R. Sheibani, Nonlocal, strain gradient and surface effects on vibration and instability of nanotubes conveying nanoflow, Mechanics of Advanced Materials and Structures, (2018) 1-13.
[33] A. Farajpour, M.H. Ghayesh, H. Farokhi, Large-amplitude parametric response of fluid-conveying nanotubes due to flow pulsations, Microsystem Technologies, (2019) 1-14.
[34] P. Malekzadeh, M. Shojaee, Surface and nonlocal effects on the nonlinear free vibration of non-uniform nanobeams, Composites Part B: Engineering, 52 (2013) 84-92.
[35] A. Farajpour, A. Rastgoo, M. Farajpour, Nonlinear buckling analysis of magneto-electro-elastic CNT-MT hybrid nanoshells based on the nonlocal continuum mechanics, Composite Structures, 180 (2017) 179-191.
[36] A. Farajpour, M.H. Ghayesh, H. Farokhi, A review on the mechanics of nanostructures, International Journal of Engineering Science, 133 (2018) 231-263.
[37] M.H. Ghayesh, A. Farajpour, A review on the mechanics of functionally graded nanoscale and microscale structures, International Journal of Engineering Science, 137 (2019) 8-36.
[38] M.H. Ghayesh, H. Farokhi, Coupled longitudinal-transverse-rotational behaviour of shear deformable microbeams, Composites Part B: Engineering, 77 (2015) 319-328.
[39] M.H. Ghayesh, Functionally graded microbeams: Simultaneous presence of imperfection and viscoelasticity, International Journal of Mechanical Sciences, 140 (2018) 339-350.
[40] H. Farokhi, M.H. Ghayesh, Supercritical nonlinear parametric dynamics of Timoshenko microbeams, Communications in Nonlinear Science and Numerical Simulation, 59 (2018) 592-605.
[41] H.-S. Shen, Nonlinear analysis of lipid tubules by nonlocal beam model, Journal of theoretical biology, 276 (2011) 50-56.

[42] J. Zhong, Y. Fu, C. Tao, Linear free vibration in pre/post-buckled states and nonlinear dynamic stability of lipid tubules based on nonlocal beam model, Meccanica, 51 (2016) 1481-1489.
[43] D. Garcia-Sanchez, A. San Paulo, M.J. Esplandiu, F. Perez-Murano, L. Forró, A. Aguasca, A. Bachtold, Mechanical detection of carbon nanotube resonator vibrations, Physical review letters, 99 (2007) 085501.

Table 1: A brief literature review on the mechanics of fluid-conveying nanotubes.

Problem	Authors	year
Mechanics of a single nanotube conveying fluid	Soltani et al. [23]	2010
Wave dispersion in a double-walled nanotube conveying fluid	Wang et al. [24]	2010
Pulsatile fluid effect on the instability of nanotubes	Liang and Su [25]	2013
Wave dispersion in fluid-conveying non-homogeneous nanotubes	Filiz and Aydogdu [26]	2015
Mechanics of fluid-conveying boron nitride nanotubes	Maraghi et al. [27]	2013
Wave dispersion in nanofluid-conveying piezoelectric nanotubes	Amiri et al. [28]	2018
Linear dynamics of fluid-conveying nanotubes	Bahaadini et al. [29]	2018
Forced vibrations of fluid-conveying nanotubes	Askari and Esmailzadeh [30]	2017
Pulsatile fluid effect on the parametric instability of nanotubes	Azrar et al. [31]	2015
Linear mechanics of nanotubes conveying fluid with stress nonlocality and strain gradient	Atashafrooz et al. [32]	2018

Table 2: Validation of the results using experimental measurement [43].

Length (nm)	Radius (nm)	Classical theory f_1 (MHz)	Size-dependent theory f_1 (MHz)	Appropriate scale parameters (χ_{nl} , χ_{sg})	Experimental measurement f_1 (MHz) **[43]**
640	1	133	36	(1.0,0.0)	30
465	0.6	155	257	(0.0,0.40)	260
572	2	329	291	(0.15,0.0)	290

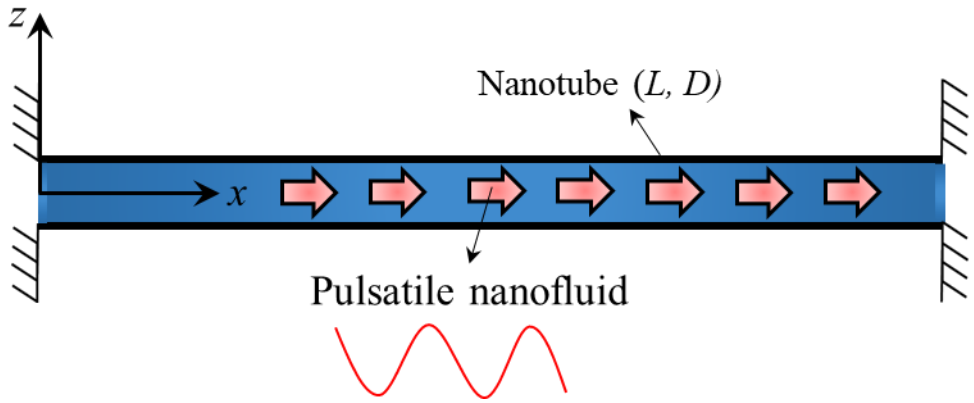

Figure 1: The schematic diagram of a viscoelastic nanotube conveying pulsatile nanofluid.

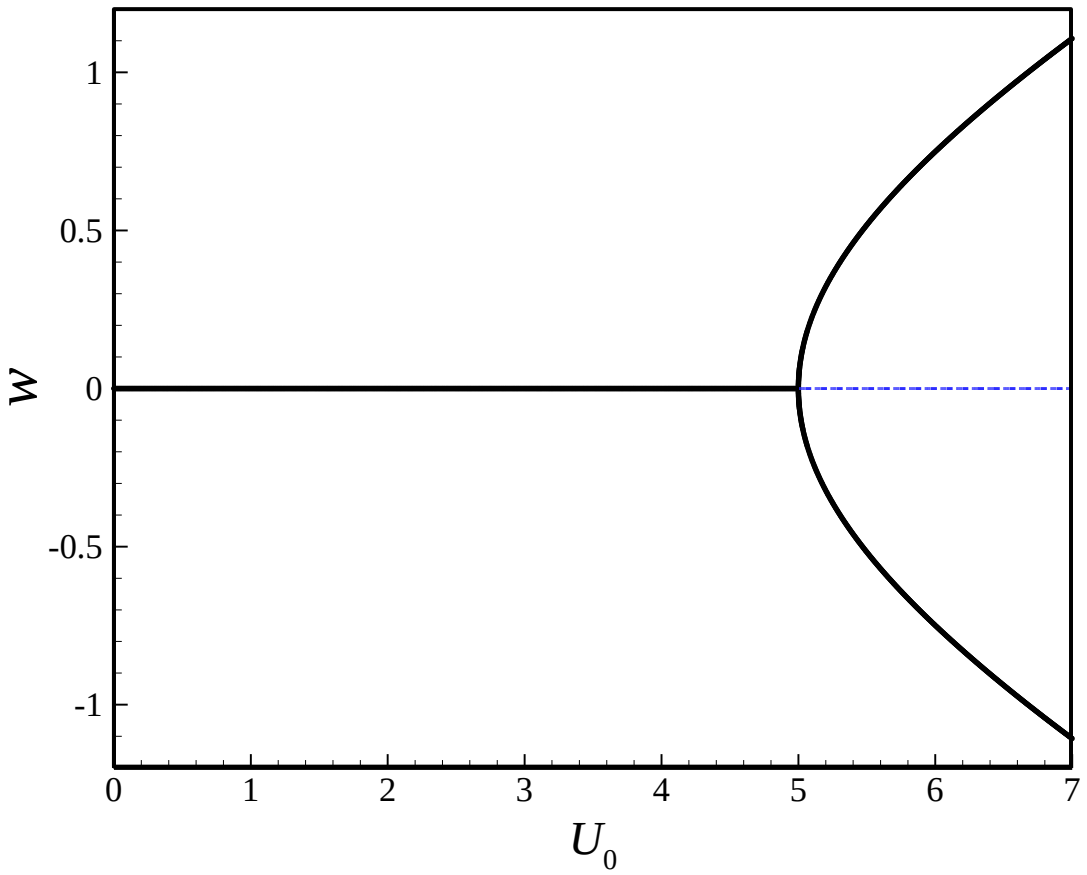

Figure 2: Bifurcation diagram of the viscoelastic nanofluid-conveying nanotube showing the transverse deflection at x=0.50. U_1= 0; dashed line shows unstable configuration.

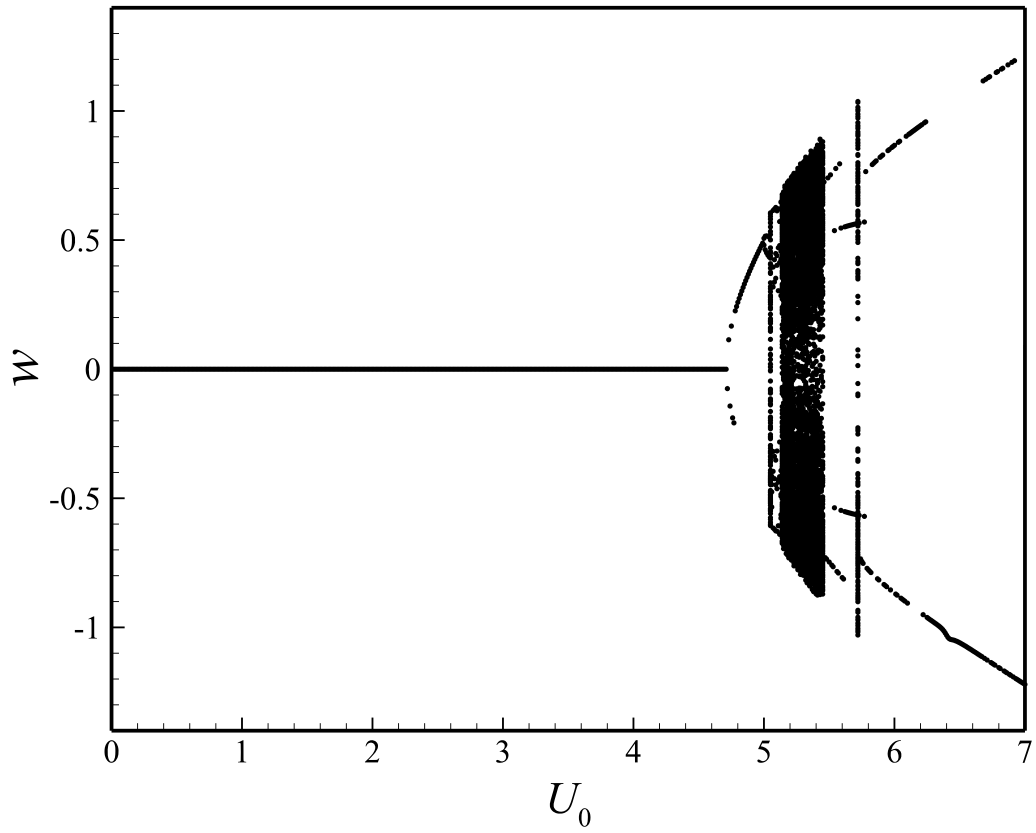

Figure 3: Bifurcation diagrams for the nonlinear transverse motion of nanotubes conveying pulsatile fluid (at x=0.50); ω_f = 5.00 and U_1= 0.05U_0.

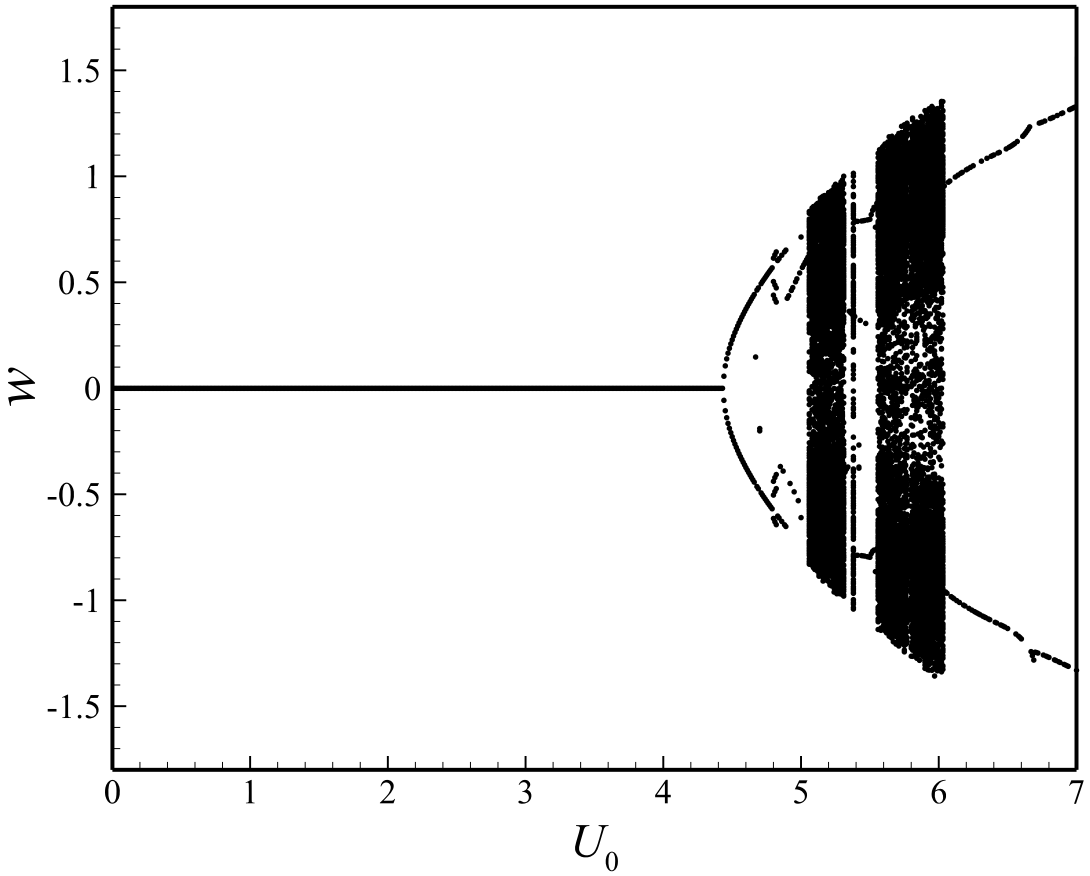

Figure 4: Bifurcation diagrams for the nonlinear transverse motion of nanotubes conveying pulsatile fluid (at x=0.50); ω_f = 5.00 and U_1= 0.10U_0.

(a)

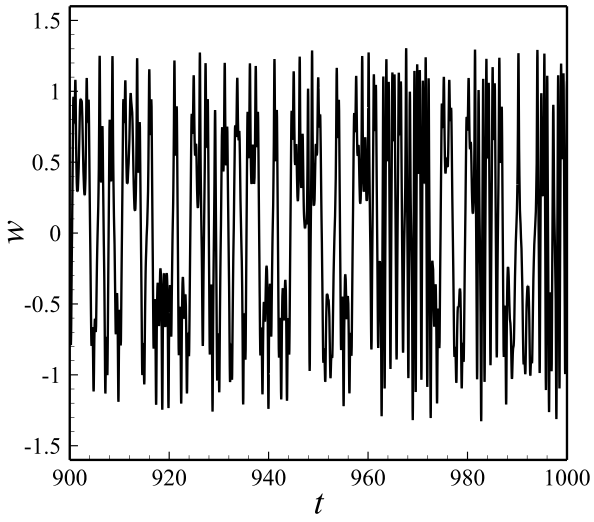
1.5
1
0.5
0
-0.5
-1
-1.5
w
900
920
940
960
980
1000
t

(b)

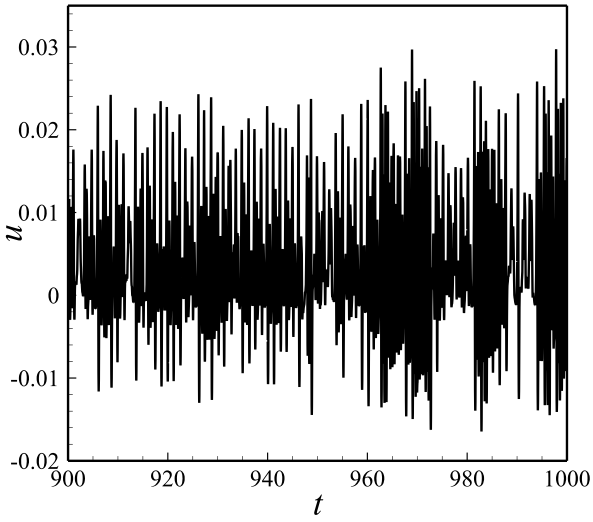
0.03
0.02
0.01
0
-0.01
-0.02
u
900
920
940
960
980
1000
t

(c)

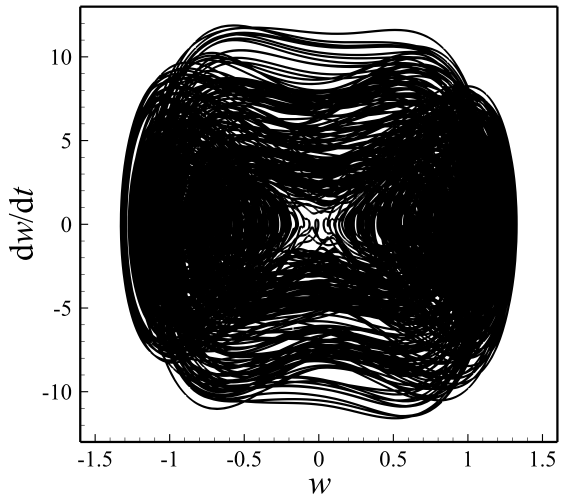
10
5
0
-5
-10
dw/dt
-1.5
-1
-0.5
0
0.5
1
1.5
w

(d)

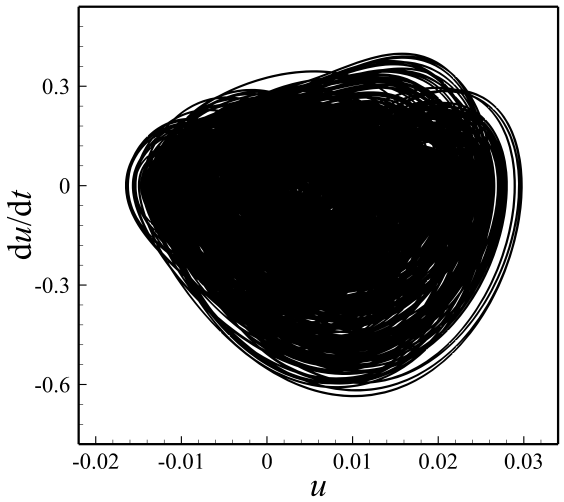
0.3
0
-0.3
-0.6
du/dt
-0.02
-0.01
0
0.01
0.02
0.03
u

(e)

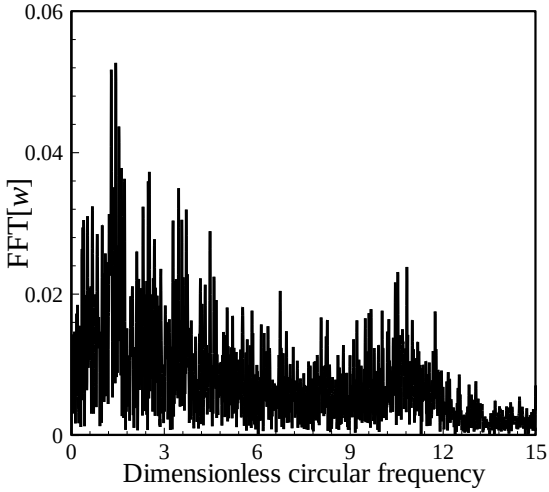
0.06
0.04
0.02
0
FFT[w]
0
3
6
9
12
15
Dimensionless circular frequency

(f)

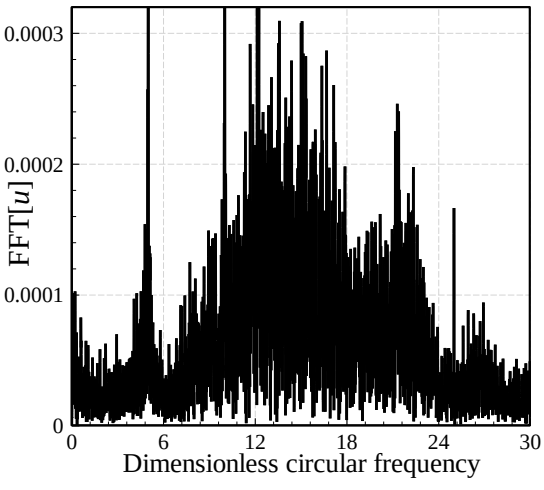
0.0003
0.0002
0.0001
0
FFT[u]
0
6
12
18
24
30
Dimensionless circular frequency

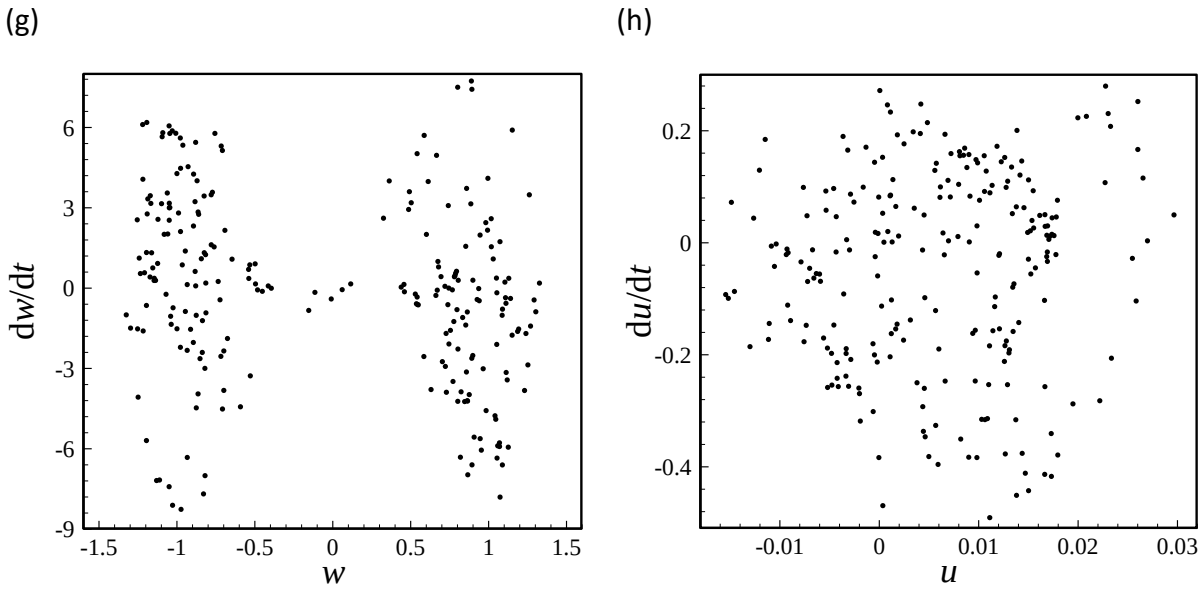

Figure 5: Chaotic motion of Fig. 4 at U_0=5.94: (a), (c), (e), and (g) time history, phase planes, FFT, and Poincaré sections for $w(x=0.5)$, respectively; (b), (d), (f), and (h) time history, phase planes, FFT, and Poincaré sections for $u(x=0.65)$, respectively.

(a)

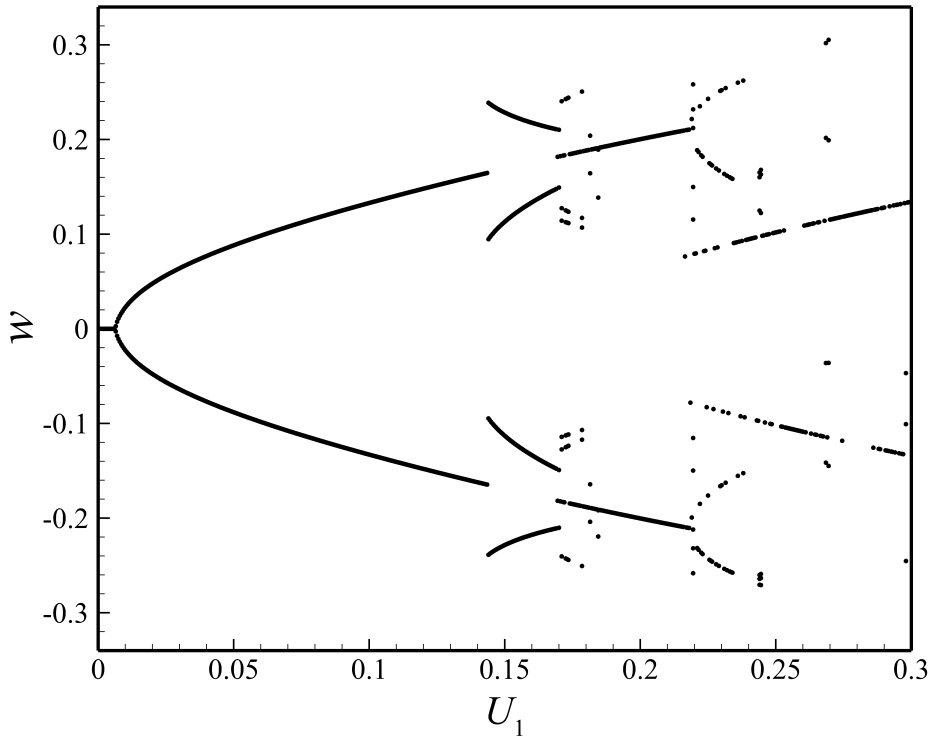

(b)

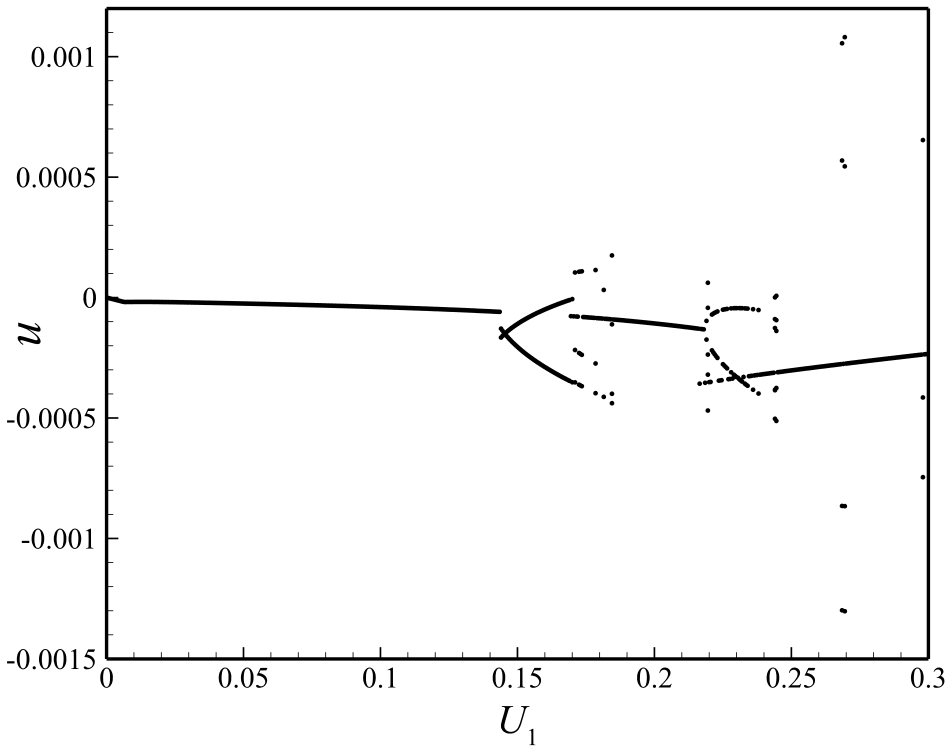

Figure 6: Subcritical bifurcations for the nonlinear motion of nanotubes conveying pulsatile fluid: (a) w(*x*=0.50); (b) u(*x*=0.65); U_0 = 4.92, ω_1= 2.9296, and ω_f/ω_1=2.0.

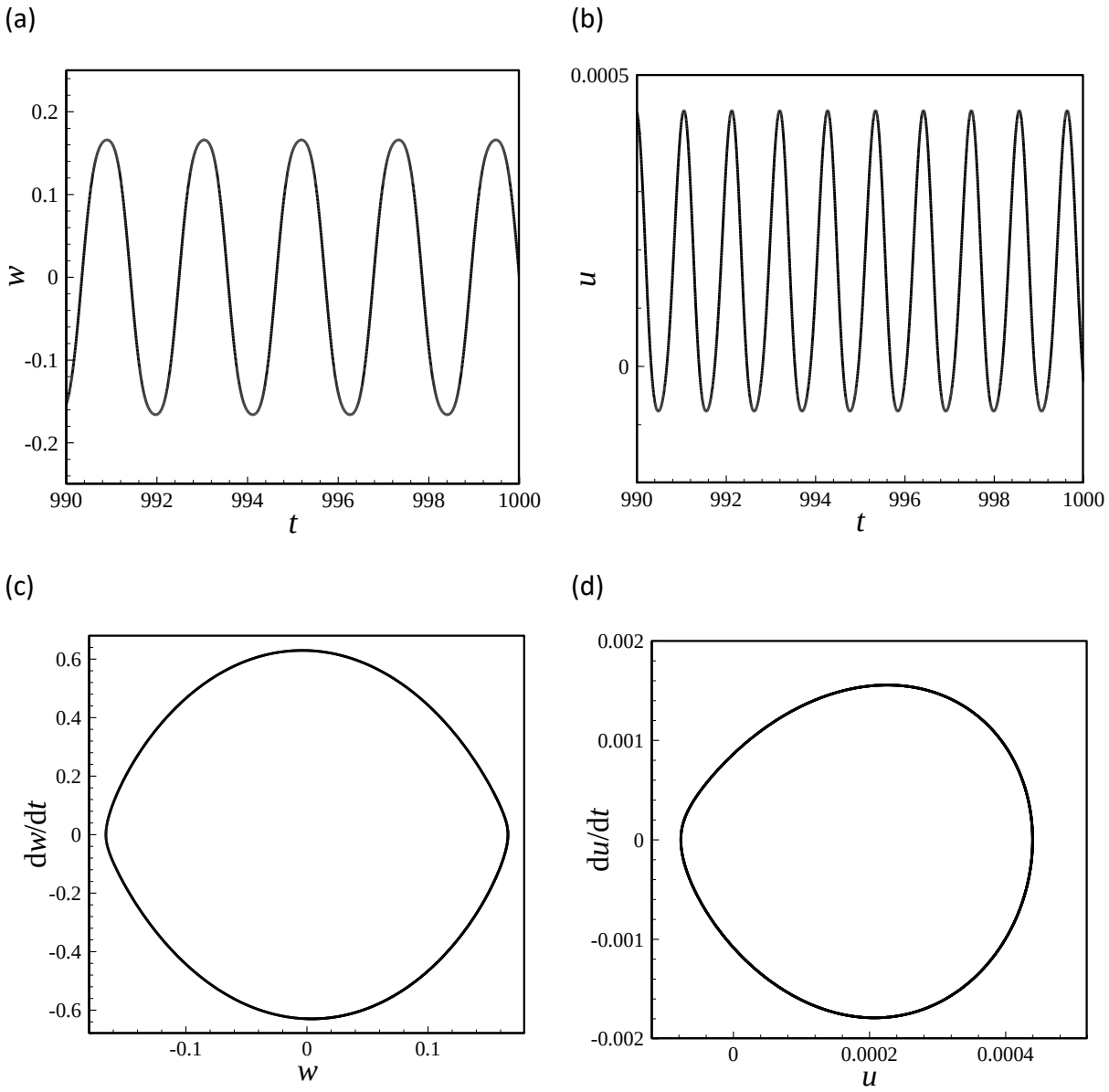

Figure 7: Period-2 motion of Fig. 6 at U_1=0.10: (a) and (c) time history and phase planes for $w(x=0.5)$, respectively; (b) and (d) time history and phase planes for $u(x=0.65)$, respectively.

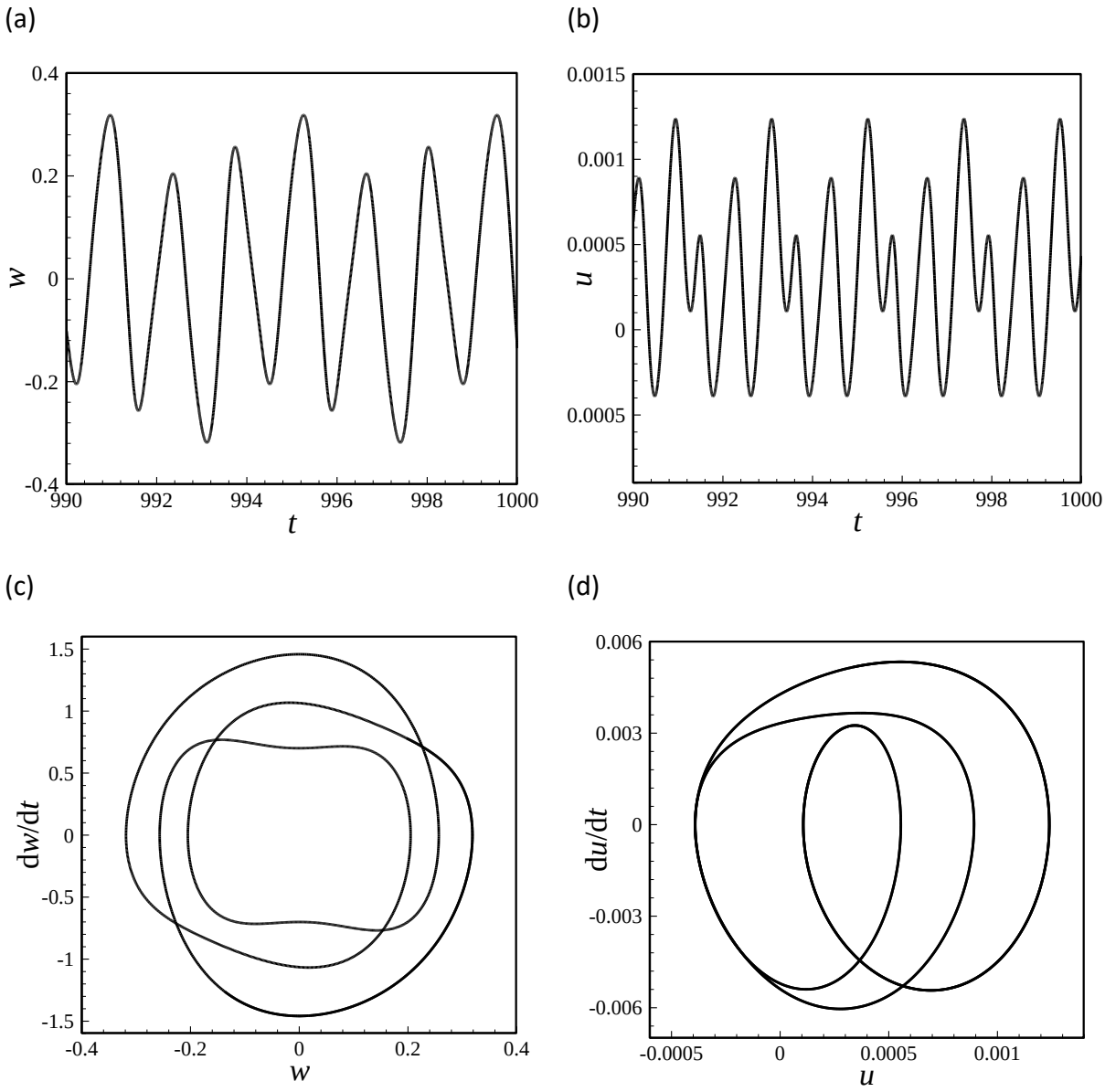

Figure 8: Period-4 motion of Fig. 6 at U_1=0.10: (a) and (c) time history and phase planes for w(x=0.5), respectively; (b) and (d) time history and phase planes for u(x=0.65), respectively.

(a)

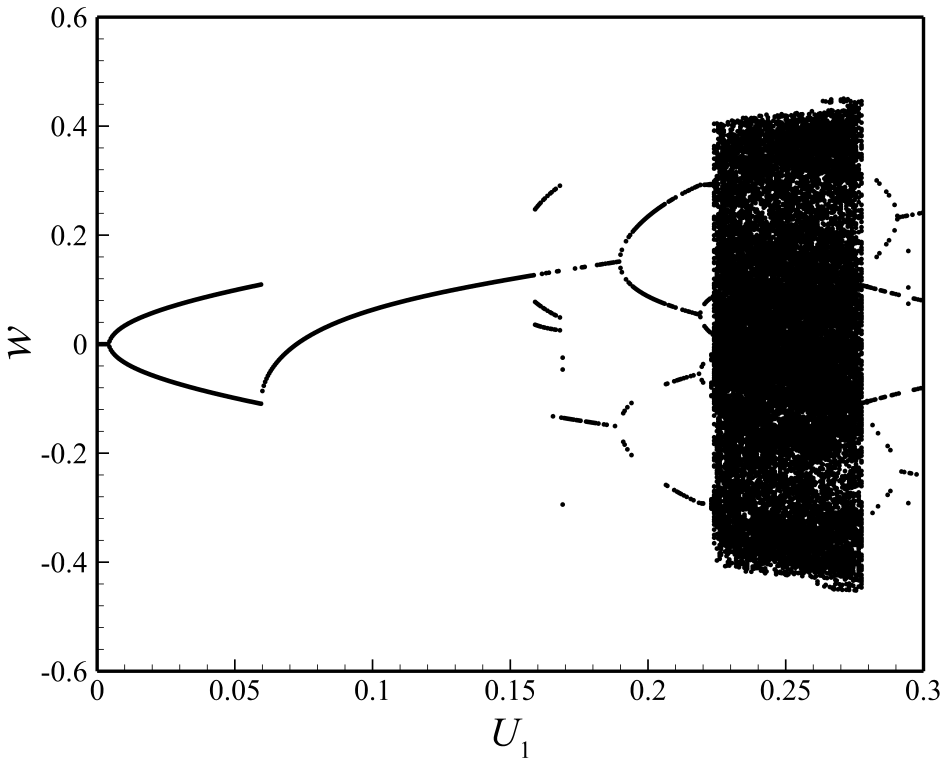

(b)

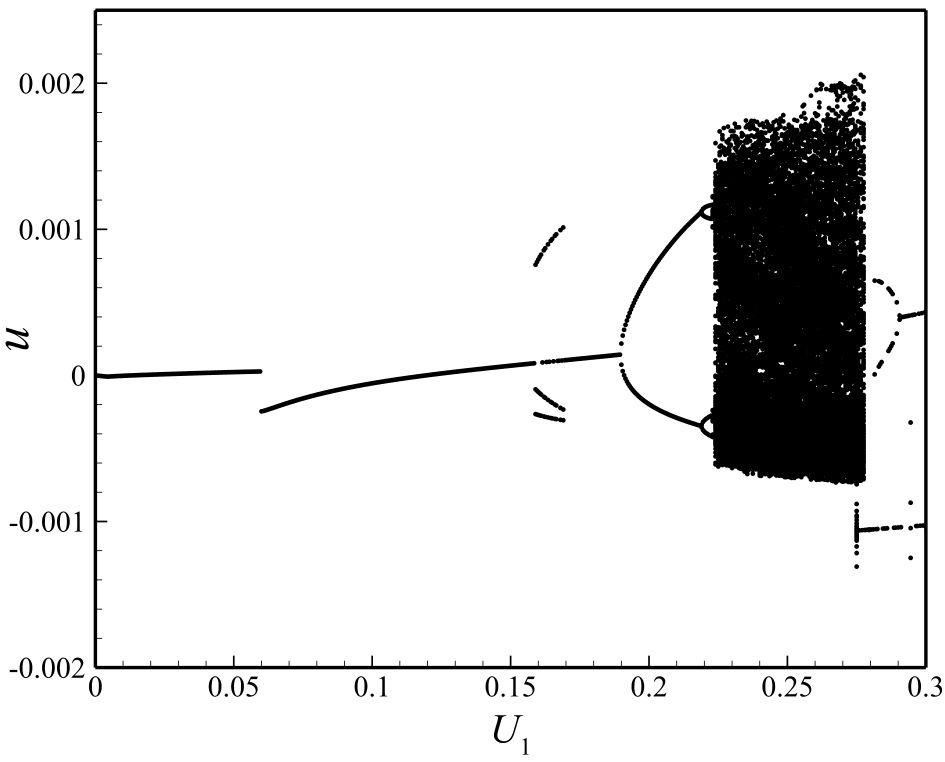

Figure 9: Subcritical bifurcations for the nonlinear motion of nanotubes conveying pulsatile fluid: (a) w(x=0.50); (b) u(x=0.65); U_0= 4.96, ω_1= 2.0590, and ω_f/ω_1=2.0.

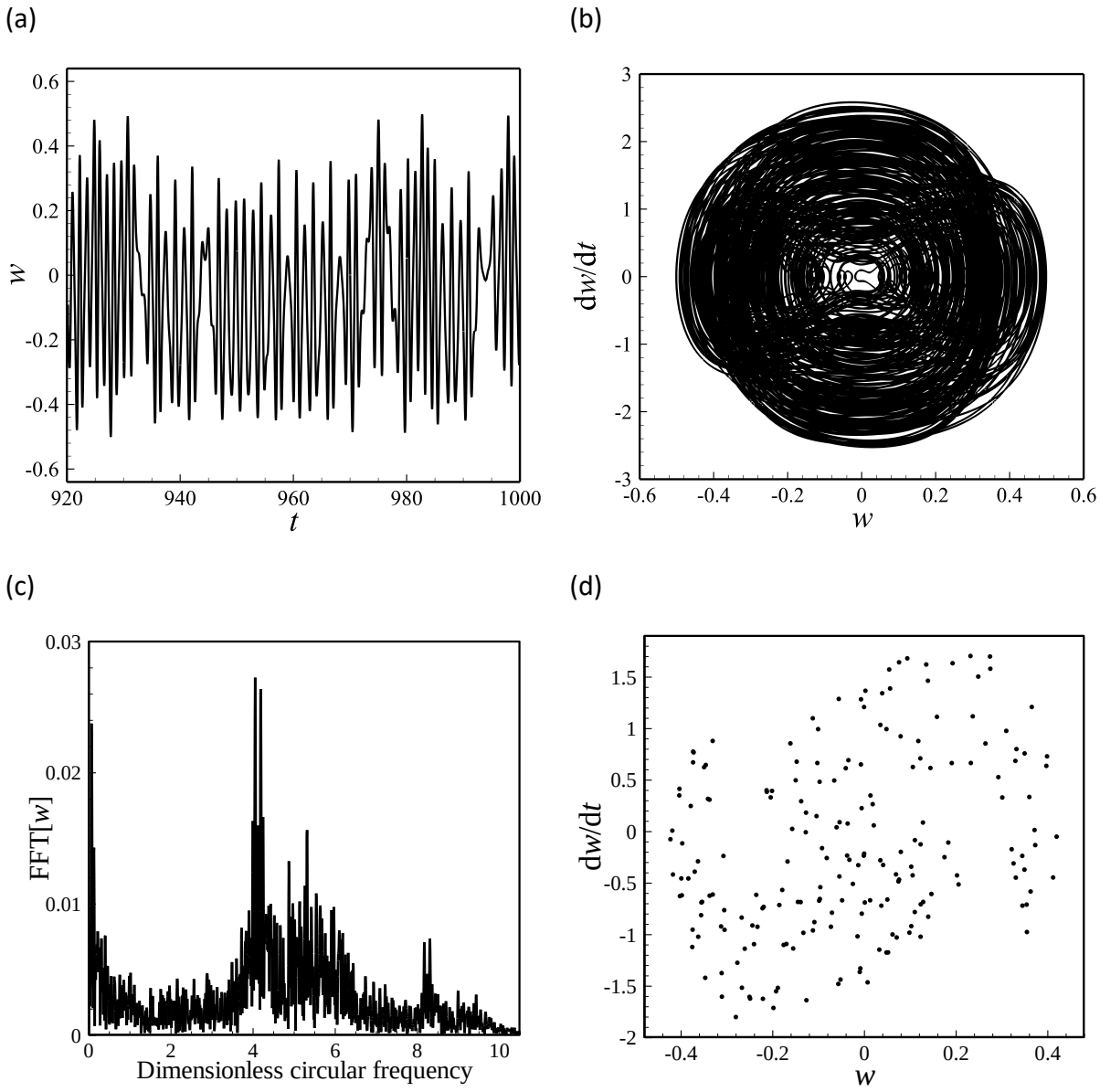

Figure 10: Chaotic motion of Fig. 9 at U_1=0.25: (a)-(d) time history, phase planes, FFT, and Poincaré section of w at x=0.5, respectively.

(a)

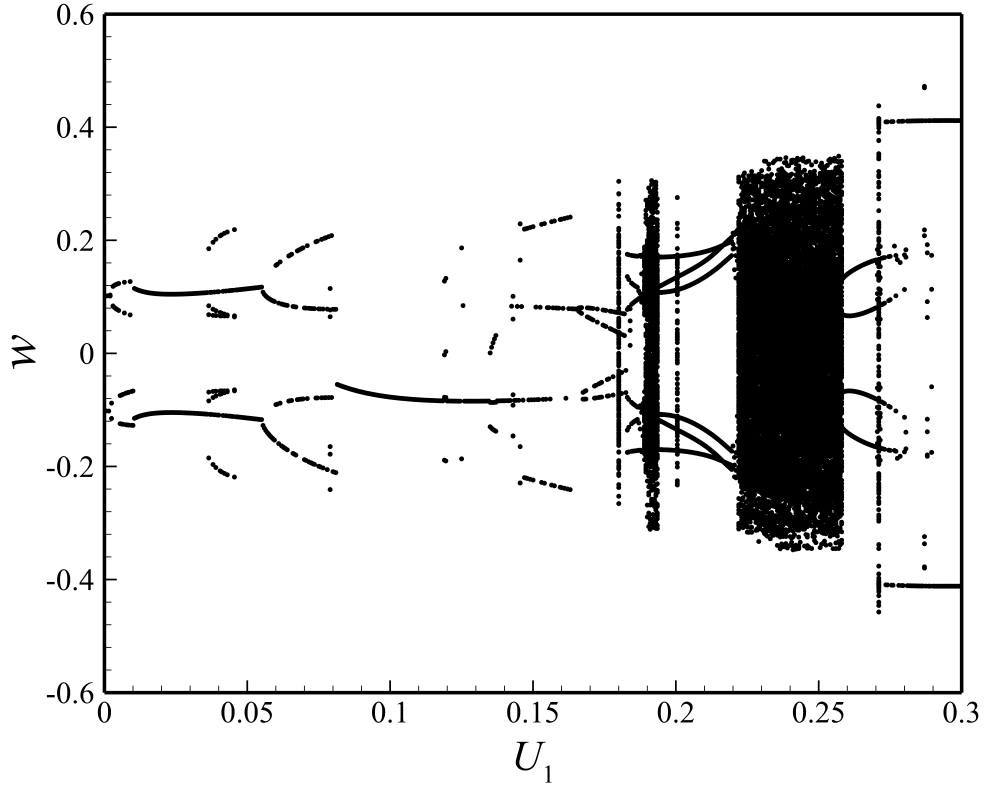

(b)

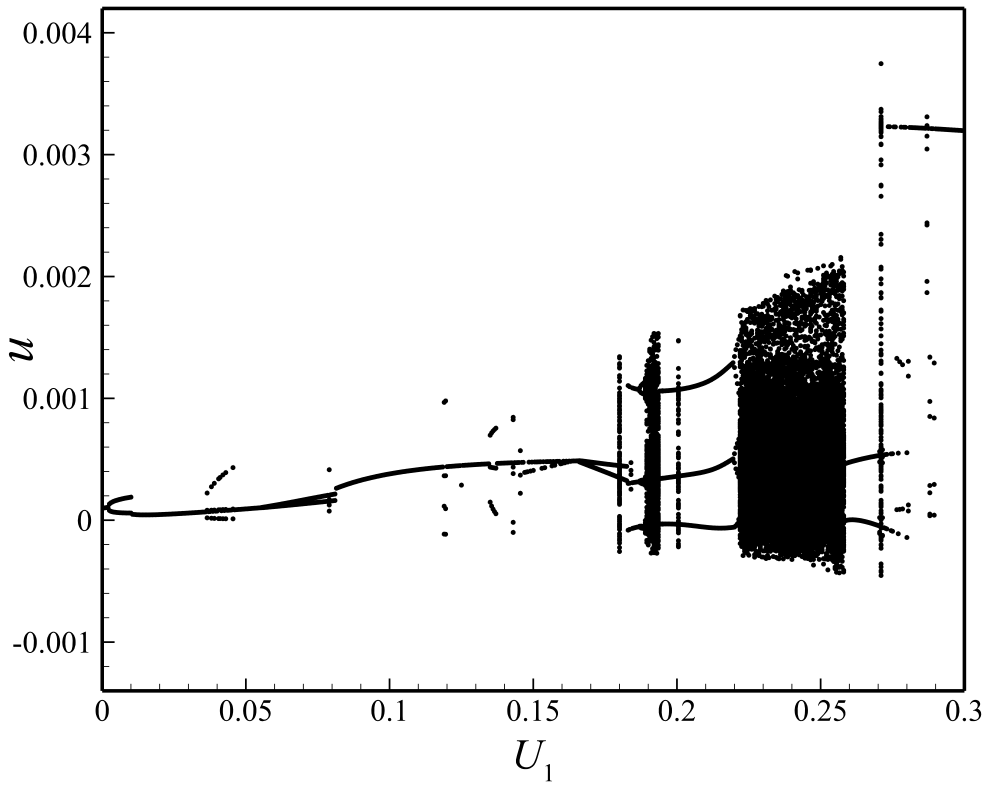

Figure 11: Supercritical bifurcations for the nonlinear motion of nanotubes conveying pulsatile fluid: (a) w(*x*=0.50); (b) u(*x*=0.65); U_0 = 5.02, ω_1= 2.0526, and ω_f/ω_1=2.0.

(a)

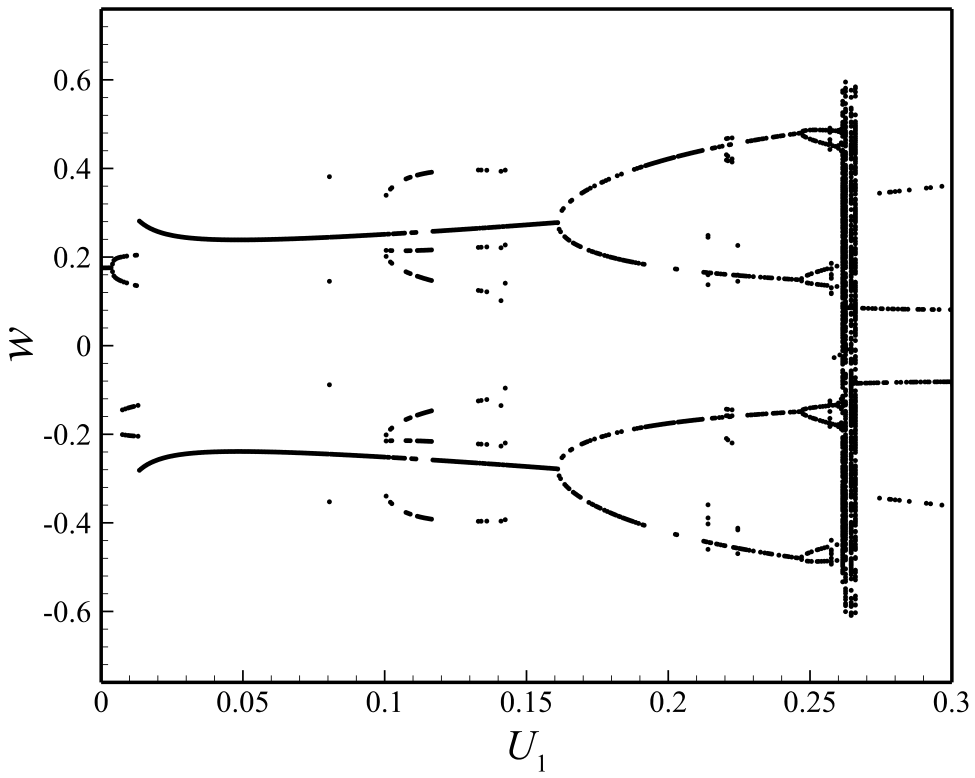

(b)

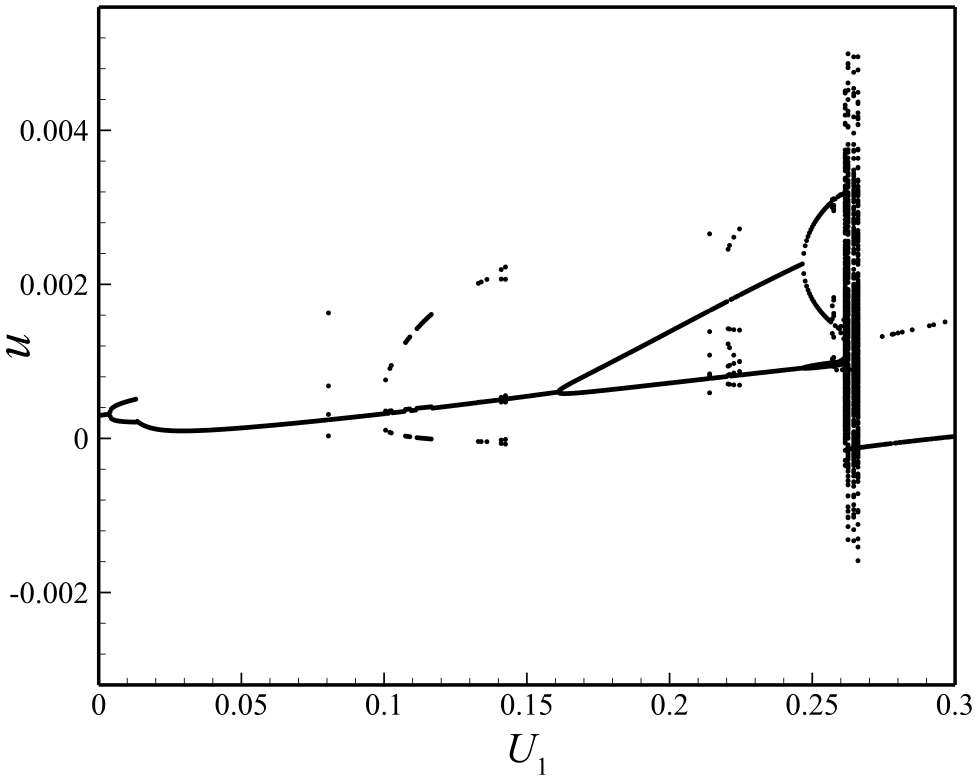

Figure 12: Supercritical bifurcations for the nonlinear motion of nanotubes conveying pulsatile fluid: (a) w(*x*=0.50); (b) u(*x*=0.65); U_0 = 5.06, ω_1= 3.5378, and ω_f/ω_1=2.0.